

This is an Open Access document downloaded from ORCA, Cardiff University's institutional repository:<https://orca.cardiff.ac.uk/id/eprint/162813/>

This is the author's version of a work that was submitted to / accepted for publication.

Citation for final published version:

Lawes, Naomi, Aggett, Kieran J., Smith, Louise R., Slater, Thomas J. A. , Dearg, Malcolm, Morgan, David J. , Dummer, Nicholas F. , Taylor, Stuart H. , Hutchings, Graham J. and Bowker, Michael 2023. Zn loading effects on the selectivity of PdZn catalysts for CO₂ hydrogenation to methanol. *Catalysis Letters* 10.1007/s10562-023-04437-5

Publishers page: <http://dx.doi.org/10.1007/s10562-023-04437-5>

Please note:

Changes made as a result of publishing processes such as copy-editing, formatting and page numbers may not be reflected in this version. For the definitive version of this publication, please refer to the published source. You are advised to consult the publisher's version if you wish to cite this paper.

This version is being made available in accordance with publisher policies. See <http://orca.cf.ac.uk/policies.html> for usage policies. Copyright and moral rights for publications made available in ORCA are retained by the copyright holders.





Zn Loading Effects on the Selectivity of PdZn Catalysts for CO₂ Hydrogenation to Methanol

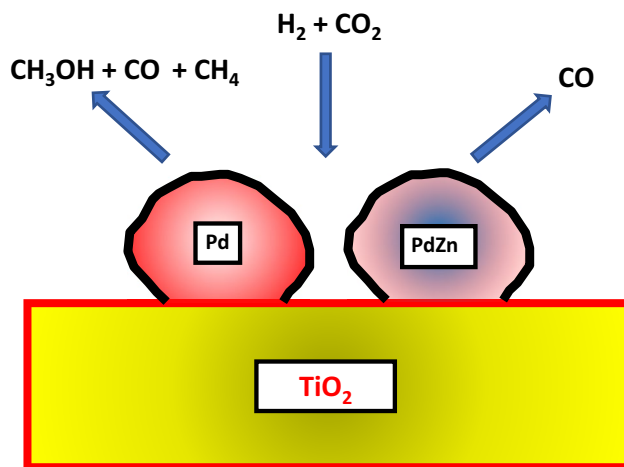
Naomi Lawes¹ · Kieran J. Aggett¹ · Louise R. Smith¹ · Thomas J. A. Slater¹ · Malcolm Dearg¹ · David J. Morgan¹ · Nicholas F. Dummer¹ · Stuart H. Taylor¹ · Graham J. Hutchings¹ · Michael Bowker^{1,2}

Received: 26 April 2023 / Accepted: 3 August 2023
© The Author(s) 2023

Abstract

PdZn/TiO₂ catalysts have been investigated for the hydrogenation of CO₂ to methanol. Varying the ratio of Pd and Zn using TiO₂ as a support has a dramatic effect on catalytic performance. Chemical vapour impregnation was used to produce PdZn alloys on TiO₂ and X-ray diffraction, X-ray photoelectron spectroscopy, and scanning transmission electron microscopy revealed changes in the structure at varying total PdZn molar ratios. Compared to monometallic Pd/TiO₂, introducing a low loading of Zn drastically changes product selectivity. When Pd is alloyed with Zn above a total Zn/Pd = 1 molar ratio, methanol selectivity is improved. Therefore, for enhanced methanol productivity, it is crucial for the Zn loading to be higher than that required for the stoichiometric formation of the 1:1 β-PdZn alloy.

Graphical Abstract



Keywords PdZn · Alloy · CO₂ hydrogenation · Methanol · Chemical vapour impregnation

✉ Michael Bowker
bowkerm@cardiff.ac.uk

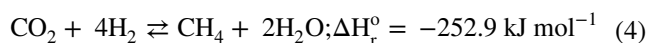
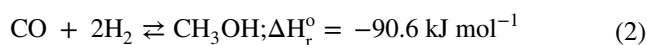
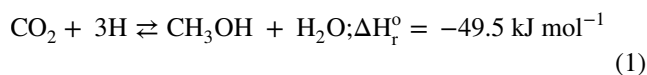
¹ Max Planck-Cardiff Centre on the Fundamentals of Heterogeneous Catalysis FUNCAT, Translational Research Hub, Cardiff University, Maindy Road, Cardiff CF24 4HQ, UK

² UK Catalysis Hub, Research Complex at Harwell, Rutherford Appleton Laboratory, Harwell, Oxon OX11 0FA, UK

1 Introduction

Interest in the catalytic hydrogenation of CO₂ in a renewable manner has accelerated in recent years due to the impact of climate change. This is especially so for industrial methanol synthesis because the source of carbon and hydrogen is usually natural gas, and considerable energy input is required to obtain the hydrogen for the reaction by the endothermic steam reforming of methane. Hence there is a need to find

a lower CO₂ emission route to methanol, using hydrogen produced from renewable energy and CO₂ obtained either from the atmosphere or from anthropogenic sources. Many researchers are investigating traditional and novel catalysts for this conversion [1, 2]. The reaction of CO₂ (Eq. 1) is intrinsically different from the current anhydrous industrial reaction (Eq. 2). The industrially used Cu/ZnO/Al₂O₃ (CZA) catalyst has been shown to deactivate when in the presence of high water content, presenting challenges for catalyst design [3–5].



Whilst supported Pd catalysts are often reported as excellent RWGS catalysts (Eq. 3), studies have shown that Pd/ZnO reduced above 300 °C result in increased methanol productivity, attributed to the formation of PdZn bimetallic nanoparticles [6]. The PdZn alloy has been found to suppress methanation (Eq. 4) when investigating Pd catalysts for methanol synthesis from CO₂ [6–8]. Methane can be detrimental during an industrial process as it accumulates in the recycle loop leading to frequent and costly purges [9], and so reducing methanation activity to low levels is important. Interestingly, the effect of different catalytic preparation methods, including chemical vapour impregnation, coprecipitation, and deposition–precipitation were investigated for CO₂ hydrogenation to methanol [7]. A linear relationship between CO₂ conversion and methanol selectivity was observed for the varying Pd/ZnO catalysts and the authors credited this to the 1:1 β-PdZn alloy formation.

We have examined the effect of varying ZnO loading on forming the alloy, by utilising TiO₂ as a support [8, 10], and so, more recently have Quilis et al. [11]. However, the preceding work used a limited range of Zn loading, only investigating loadings at and above that required for the stoichiometric formation of the 1:1 β-PdZn alloy. Furthermore, van Bokhoven and co-workers indicated the importance of ZnO in addition to the β-PdZn alloy, whereby ZnO facilitates CO₂ adsorption, and the alloy can enable hydrogen spillover [12]. Considering the importance of alloy formation, the critical question about catalyst performance at low Zn loadings remains unanswered. We have now addressed this important question and here we report results for lower amounts of Zn, including those below that needed for the complete formation of the 1:1 β-PdZn alloy, and show that this affects the selectivity in a rather remarkable way.

2 Experimental Section

2.1 Materials

The following chemicals and reagents were purchased from Sigma Aldrich; palladium acetylacetonate (Pd(acac)₂, 99%), zinc acetylacetonate (Zn(acac)₂, 99%), ZnO (99.9%, nanopowder, < 100 nm particle size), TiO₂ (P25, Evonik). The chemicals were used as provided without further purification.

2.2 Chemical Vapour Impregnation (CVI) Synthesis

Catalysts were prepared using CVI with a fixed Pd loading of 5 wt%. The procedure for preparing 2 g of 5 wt% PdZn/TiO₂ (Zn/Pd molar ratio of 0.5) Pd(acac)₂ (9.4 × 10⁻⁴ mol), Zn(acac)₂ (4.7 × 10⁻⁴ mol) and TiO₂ (1.87 g) were physically mixed in a glass vial for 1 min. The mixture was transferred to a Schlenk flask and sealed. The tube was connected to a Schlenk line and evacuated (~ 10⁻³ mbar). The tube was lowered into an oil bath preheated to 80 °C and the temperature was increased to 133 °C and maintained for 1 h. The material was then recovered and calcined in static air (500 °C, 5 °C min⁻¹, 16 h). For PdZn/TiO₂, various ratios of Pd:Zn are denoted Pd_xZn_y/TiO₂, referring to a Zn/Pd molar ratio of y/x.

2.3 CO₂ Hydrogenation Catalyst Testing

Catalytic testing for CO₂ hydrogenation was carried out using a 16-bed high throughput catalytic reactor, designed, and manufactured by Integrated Lab Solutions GmbH (ILS). Integrated Workflow manager, based on LabView, was used to operate the reactor, and was automated using Siemens Win CC software. The high throughput reactor operates all beds under the same reaction conditions and has a fixed bed, continuous flow design. Equilibrar back pressure regulators controlled the pressure in each bed, and gases were fed through a capillary distribution system. To control and measure the reaction temperature, a thermocouple was positioned inside each of the four heating blocks, containing four beds each. Stainless steel reactor tubes with an internal diameter of 4.57 mm were used. Catalysts were pelleted (0.5 g, 425–600 μm), mixed with F80 silicon carbide (mean particle size 190 μm) and were supported on a bed of F24 silicon carbide (particle size 750 μm) to limit mass transfer and to ensure the sample was in the centre of the isothermal zone. Prior to testing, the catalysts were reduced in situ in a flow of 5% H₂/N₂ gas (400 °C, 1 h, 5 °C min⁻¹) and subsequently cooled to 125 °C under N₂. The gas composition was switched to the reactant gas (22% CO₂, 54% H₂, 5% Ar,

19% N₂), with a flow rate of 30 mL min⁻¹ at atmospheric pressure. The system was then pressurised to 20 bar using the gas feed pressure over the Equilibar back pressure regulator and left to stabilise for 4 h. Reaction was conducted at 230 °C, and to stop any products condensing in the reactor lines, the downstream oven was set to 120 °C. To limit product build-up in the downstream reactor lines, a purge feed of nitrogen, equivalent to the reaction, feed was used. The gaseous products were analysed via online gas chromatography (Agilent 7890B system with two flame ionisation detectors and a thermal conductivity detector). Argon was used as an internal standard. Four injections were taken at each temperature per reactor, and the Vici stream selection valve was switched between the beds to allow sampling of the products. From the moles of CO₂ in the calibration at 125 °C compared to the moles of CO₂ at each temperature for each bed, CO₂ conversion was calculated. Methanol, methane, and CO were the main products observed. The carbon balance was calculated using the sum of carbon containing products and reactants in the feed divided by the sum of carbon containing reactants in the calibration runs. Catalyst testing errors were calculated by running 12 commercial Cu/ZnO/Al₂O₃ (CZA) standards using conditions stated.

2.4 Catalyst Characterisation

Powder X-ray diffraction (XRD) patterns were measured on a PANalytical X'pert Pro powder diffractometer operating at 40 kV, 40 mA using Cu K α radiation ($\lambda = 1.54 \times 10^{-10}$ m) with a Ge (111) single crystal monochromator. The International Centre for Diffraction Data database was used as a reference to assign phases present.

Inductively coupled plasma mass spectroscopy (ICP-MS) was performed to quantify total metal loading. The metal catalysts were digested (10 mg of catalyst, 1 mL of aqua regia, 24 h), filtered and diluted to a metal concentration of about 10 ppm. Metal concentrations were determined using an Agilent 7900 ICP-MS with an I-AS autosampler.

X-ray photoelectron spectra (XPS) were recorded on a Kratos Axis Ultra-DLD photoelectron spectrometer, utilising monochromatic Al K α radiation operating at 150 W power (10 mA \times 15 kV). All spectra were recorded using a pass energy of 40 eV and step size of 0.1 eV for high resolution spectra, whilst survey spectra were recorded using a pass energy of 160 eV. All samples were mounted for analysis by pressing onto silicone free double sided adhesive tape attached to a glass slide to allow isolation from the spectrometer. All data were acquired using a magnetically confined electron only charge compensation system and charge corrected to the C 1s signal at 284.8 eV. Transmission corrected XPS data were analysed using Casa XPS software (v2.3.26 PR1.0N) after subtraction of Shirley background

and using modified Wagner sensitivity factors as supplied by the instrument manufacturer [13].

Transmission electron microscopy (TEM) and scanning transmission electron microscopy (STEM) were performed on a JEOL JEM-2100 operating at 200 kV. Energy dispersive X-ray analysis (EDX) was done using an Oxford Instruments X-MaxN 80 detector and the data analysed using the Aztec software. Samples were deposited on 300 mesh copper grids coated with holey carbon film. TEM and STEM were also performed on a TF Spectra 200 operating with an acceleration voltage of 200 kV. STEM was also performed using a JEOL ARM200F microscope at the electron Physical Sciences Imaging Centre at Diamond Light Source. An acceleration voltage of 200 kV, a convergence semi-angle of 23 mrad and a high-angle annular dark field (HAADF) inner angle of 80 mrad were used for data collection. EDX spectrum imaging was performed using a JEOL Centurio dual detector. Samples were subsequently also imaged using a probe-corrected 200 kV Thermo-Scientific Spectra 200 Scanning Transmission Electron Microscope, at an accelerating voltage of 200 kV and with a convergence semi-angle of 30 mrad. The HAADF detector had an inner collection angle of approximately 56 mrad (outer angle approximately 200 mrad). EDX spectrum images were acquired on a Super-X detector using all four detectors.

3 Results and Discussion

3.1 Catalytic Activity

We have investigated methanol synthesis from CO₂ hydrogenation on Pd and PdZn alloy catalysts supported on TiO₂. The catalysts were made by a solvent free deposition technique, referred to as chemical vapour impregnation (CVI), and calcined, followed by a reduction step prior to catalytic testing. Bowker et al. has shown previously that CVI is an excellent method for making small, stable PdZn nanoparticles [7]. Figure 1a shows the overall trend of methanol productivity at 230 °C with increasing Zn content. Interestingly, methanol productivity decreases at low Zn/Pd ratios, but once the equimolar ratio is exceeded, a sharp rise in methanol productivity is observed at Zn/Pd ratios of 1.5 and 2.0. As Fig. 1b illustrates, when there is no Zn added to the system, the Pd/TiO₂ catalyst produces three dominant products and these are, in order of abundance, CO > CH₄ > CH₃OH (54%, 26%, 20%, respectively), see Table 1. However, as the loading of Zn in the system increases, the pattern of reactivity changes considerably. It has previously been shown that Pd can alloy with Zn to make a 1:1 β -PdZn alloy [6, 7, 14–16]. However, even with insufficient Zn to complete this alloy, at 0.1 ratios of Zn/Pd, the methanation selectivity has dropped considerably

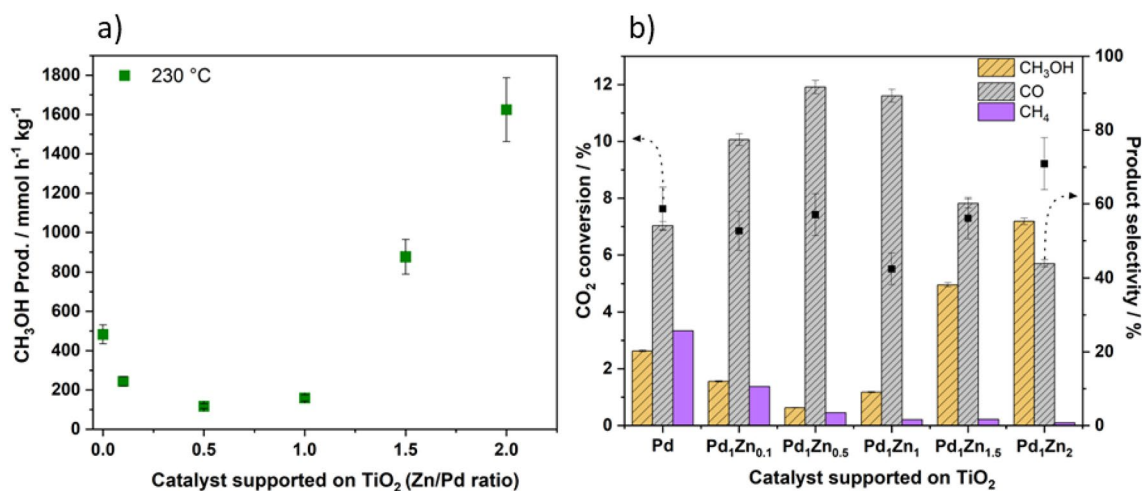


Fig. 1 **a** Methanol productivity as a function of varying Zn/Pd ratios supported on TiO₂ for CO₂ hydrogenation. **b** CO₂ conversion and product selectivity to CH₃OH as a function of varying Zn/Pd ratios

supported on TiO₂. 0.5 g catalyst, pre-reduced in situ (5% H₂/Ar, 400 °C, 1 h, 5 °C min⁻¹) and run at 230 °C, 20 bar, 30 mL min⁻¹. Pd loading fixed at 5 wt%

Table 1 Product selectivity at 230 °C

Catalyst supported on TiO ₂	Product selectivity/%		
	CH ₃ OH	CO	CH ₄
Pd	20	54	26
Pd ₁ Zn _{0.1}	12	77	11
Pd ₁ Zn _{0.5}	5	92	3
Pd ₁ Zn ₁	9	89	2
Pd ₁ Zn _{1.5}	38	60	2
Pd ₁ Zn ₂	55	44	1

Table 2 Elemental analysis by ICP-MS

Catalyst	Intended Pd loading/wt%	Actual Pd loading/wt%	Intended Zn loading/wt%	Actual Zn loading/wt%
Pd/TiO ₂	5	5.0	0	0
Pd ₁ Zn _{0.1} /TiO ₂	5	5.2	n.a	n.a
Pd ₁ Zn _{0.5} /TiO ₂	5	5.3	1.54	1.5
Pd ₁ Zn ₁ /TiO ₂	5	5.7	3.07	3.3
Pd ₁ Zn _{1.5} /TiO ₂	5	5.8	4.61	4.4
Pd ₁ Zn ₂ /TiO ₂	5	5.7	6.14	7.2

from 26% down to 11%, and for the 0.5 ratio it decreases to 3%. Methanol formation similarly diminishes at low ratios of Zn/Pd, from around 20% selectivity with no Zn present to a minimum of around 5%, but then increases again at higher Zn/Pd ratios to a maximum of ~55%. Of course, the corollary of this is that CO increases to a maximum selectivity of 92% at a 0.5 ratio. It is likely that CO is the source of methanation, as at low Zn ratios, a decrease in methane is accompanied by increasing CO selectivity. It is known from the literature to be methanated at these temperatures [17–20], and CO₂ itself is only weakly bound on Pd, much more weakly than CO [12]. Above a Zn/Pd ratio of 0.5, methanol increases with increasing Zn, and CO diminishes to 44% at Zn/Pd ratio of 2. CO is the main product until the Zn/Pd ratio exceeds 1, and it is likely to be formed on the metal, and then desorb as part of the RWGS reaction [18, 21]. CO, however, can further hydrogenate and produce methane [18], as seen with Pd/TiO₂. But when Zn is incorporated, CO dissociation appears to be blocked, and we observe a decrease in methane selectivity on all Pd_xZn_y/TiO₂ catalysts (Table 1). Gallagher et al. [22] proposed

that the size reduction of the Pd ensemble affects the binding strength of CO and a shift from bridge binding to terminal binding is observed, therefore CO is more likely to desorb rather than further hydrogenate. During all these changes, although there is significant selectivity variation, there is relatively little variation in conversion, starting at 7.7(±0.7)% with no Zn present, reducing to 5.5(±0.7)% at a Zn/Pd ratio of 1, then rising again to 9.1(±1.0)% at the highest ratio of Zn/Pd = 2. The decrease up to a ratio of 1 may be due to the presence of Zn at the surface of the Pd nanoparticles, whereas the increase above that ratio is due to the presence of ZnO in the sample.

3.2 Elemental Analysis

The content of Pd and Zn in the catalysts were determined by ICP-MS, as presented in Table 2. The catalyst weight loadings are generally close to that expected, except for the highest loading which had a little more Zn than aimed for.

3.3 Electron Microscopy

HAADF STEM images and EDX elemental maps were used to indicate the extent of alloying over the PdZn samples in this study (Fig. 2). Formation of the 1:1 PdZn alloy was expected for the higher ratios, as shown in previous work whereby Zn reacts with Pd during reduction to form the 1:1 β -PdZn alloy [6]. It has also been shown by Bowker et al. that PdZn nanoparticles formed on Pd/ZnO are stable post reaction: the PdZn average particle size was 3.5 nm and within experimental error no change was seen in size distribution after CO₂ hydrogenation [7]. Even though at low ratios (< 1:1) the Pd nanoparticles cannot be saturated with Zn, nonetheless it is clear from Fig. 2a that there is preferential location of the Zn at the Pd particles. The alloy is essentially complete by Zn/Pd = 1 (Fig. 2c).

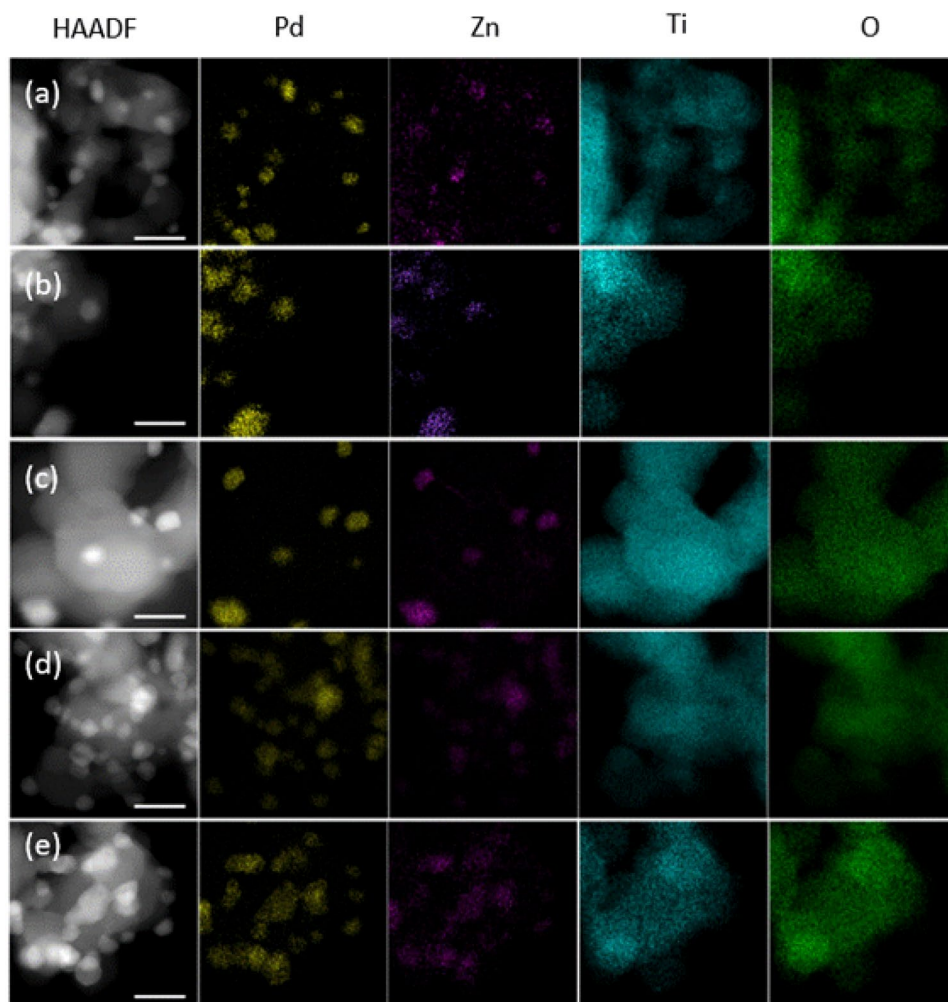
Particle sizes of Pd and PdZn nanoparticles were measured using a combination of TEM and HAADF-STEM images. Fig. S1 shows the TEM, HAADF-STEM images, and particle size distribution histograms for reduced Pd/TiO₂ and Pd_xZn_y/TiO₂ catalysts. It has previously been reported

that Pd nanoparticles via CVI result in narrow particle sizes and distributions [9, 23]. We observe average particle sizes ranging from 4.3 to 7.5 nm but there is no clear trend relative to change in composition, the mode usually being around 6 nm. Within experimental certainty, variations in methanol productivity are not related to changes in particle size, and hence changes in metal surface area. This implies the amount of available ZnO, rather than metallic Zn in the alloy, is the key factor for the observed shift from the RWGS reaction to methanol formation.

3.4 X-ray Diffraction

The formation of PdZn has been investigated by XRD, as seen in Fig. 3. The samples were analysed after reduction at 400 °C. For Pd/TiO₂, Pd metal is observed at 40.2° in addition to TiO₂ reflections. At the 0.5 ratio, a significant reduction in the Pd peak at 40.2° is observed. The PdZn peaks at 41.3° and 44.3° are unfortunately obscured by rutile TiO₂ peaks, but by Zn/Pd = 1.5 and above, they are clearly present. However, when comparing the TiO₂ reflections, at

Fig. 2 HAADF-STEM imaging and EDX elemental mapping for **a** Pd₁Zn_{0.1}/TiO₂, **b** Pd₁Zn_{0.5}/TiO₂, **c** Pd₁Zn₁/TiO₂, **d** Pd₁Zn_{1.5}/TiO₂ and **e** Pd₁Zn₂/TiO₂ after reduction at 400 °C, 5% H₂/Ar. Each scale bar in HAADF imaging represents 20 nm



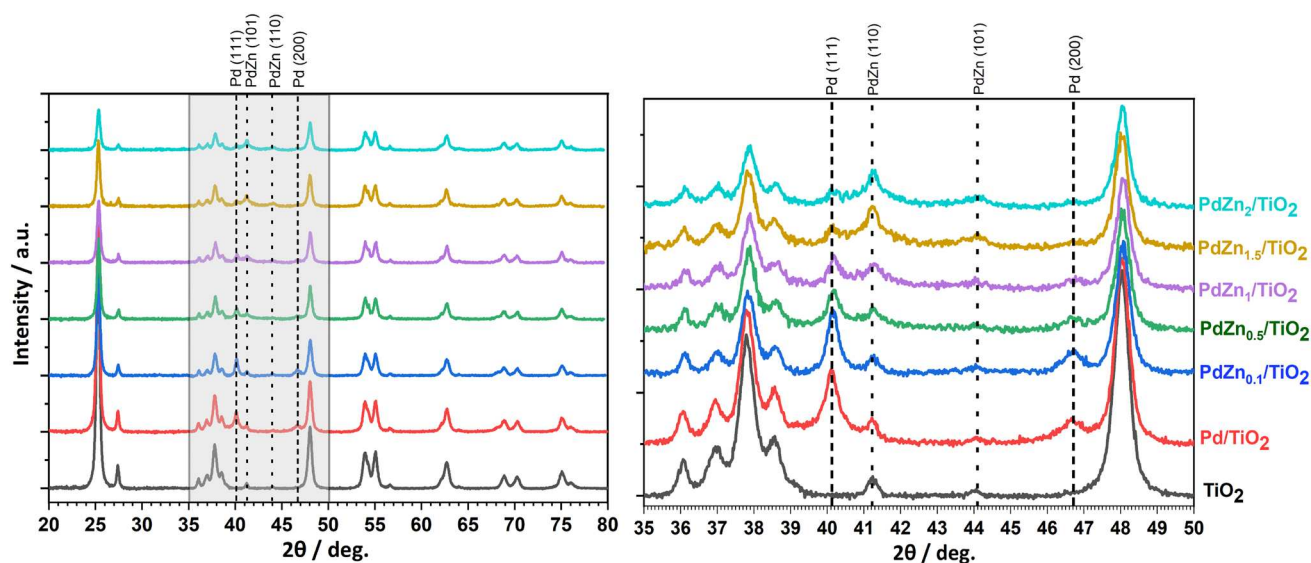


Fig. 3 X-ray diffraction patterns of P25 TiO_2 , Pd/TiO_2 , and varying Zn/Pd ratios of PdZn/TiO_2 samples. All catalysts were reduced prior to characterisation (400°C , 1 h, 5% H_2/Ar). The right hand panel is an expanded version of the shaded area in the left panel

Zn/Pd = 0.5, the ratio of the 41.3° peak to the main TiO_2 peak at 37.8° has increased by approximately a factor of two, indicating PdZn presence is likely even at this ratio. Furthermore, the PdZn peak does not measurably shift with increasing Zn loading, showing it remains the 1:1 β -PdZn alloy. At these ratios, ZnO reflections are not expected to be observable, however, it is expected that ZnO will be present, as at Zn/Pd 1.5 and 2, the loadings are above that required for the stoichiometric formation of the 1:1 β -PdZn alloy. However, it is difficult to observe a thin layer of ZnO by XRD. Further, we cannot rule out that there may be dilute amorphous alloy phases.

3.5 X-ray Photoelectron Spectroscopy

To further investigate the formation of the PdZn alloy nanoparticles, XPS was used to allow for surface-specific analysis (Fig. 4). PdZn/TiO_2 at Zn/Pd ratios 0.1, 0.5, 1, and 1.5, were reduced in 5% H_2 at 400°C for 1 h prior to analysis. Presence of both Pd metal and Pd alloy were observed, similar to that seen in XRD. The Pd 3d peak was measured at 334.9 eV, corresponding to Pd metal, and at 335.9 eV for the PdZn alloy. Even at a low Zn/Pd ratio of 0.1, some PdZn alloy is starting to be formed. The PdZn peak intensity increases as the loading of Zn increases. The alloy binding energy is in line with the 1:1 β -PdZn alloy, and so we conclude that the alloy forms as a two-phase system of Pd and 1:1 PdZn, with the latter increasing as Zn loading increases. Since there is already a dramatic reduction in methane production at this low loading, we also conclude that there is preferential segregation of Zn to the surface region. Segregation is related to a number of factors, but surface energy is perhaps the most

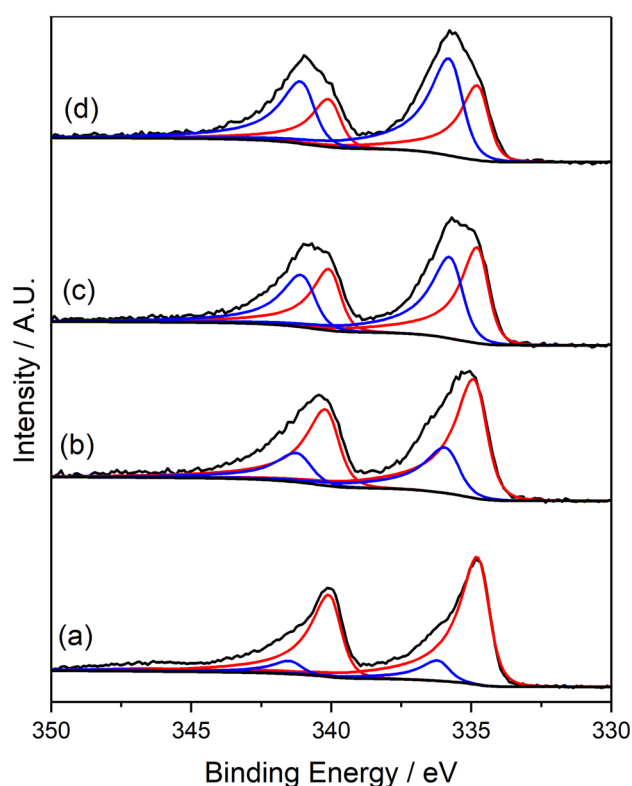


Fig. 4 Pd 3d XPS spectra for the catalysts with varying Pd ratio. Zn/Pd ratios are **a** 0.1, **b** 0.5, **c** 1, **d** 1.5. Pd and PdZn in the peak fitting are represented by the red and blue lines, respectively, and the black solid line represents the recorded spectra

important. Since the surface energy of Zn (0.32 J m^{-2}) is so low compared with Pd (1.51), then it will tend to segregate to the surface region [24]. Further confirmation of the presence of Zn metal is given in the X-ray Auger electron spectra (XAES) in the supporting information, Fig. S2.

4 Conclusions

Studying low loadings of Zn in a PdZn/TiO₂ catalyst indicates that when varying Zn loading, from Zn/Pd ratios of 0.1 up to 2, a dramatic effect on catalytic performance is observed. Monometallic Pd supported on TiO₂ is a RWGS catalyst with significant methane production (25% selectivity), but Pd₁Zn₂/TiO₂, has < 0.8% methane selectivity and methanol selectivity of 55%. The presence of the 1:1 β-PdZn alloy begins to form at a Zn/Pd ratio as low as 0.1. Interestingly, Pd₁Zn₁/TiO₂ shows the highest levels of CO, but above this ratio of Zn to Pd greatly increased methanol selectivity is observed due to the presence of ZnO. Clearly an excess of ZnO is important for methanol synthesis.

Supplementary Information The online version contains supplementary material available at <https://doi.org/10.1007/s10562-023-04437-5>.

Acknowledgements We thank Diamond Light Source (Instrument E01 and proposal numbers MG27530 and MG31044), and the EPSRC grant EP/V029797/2 for the support of the electron microscopy. We would like to thank the CCI Electron Microscopy Facility which has been part-funded by the European Regional Development Fund through the Welsh European Funding Office, and The Wolfson Foundation. We thank the Max Planck Society and Cardiff University for financial support to create the FUNCAT Centre. The authors wish to acknowledge support from the EPSRC International Centre-to-Centre Project: new trimetallic nanoparticles as catalysts for the conversion of carbon dioxide to renewable fuels (EPSRC EP/S030468/1). We also thank the UK Catalysis Hub, funded through EPSRC Grants EP/R026939/1 and EP/R026815/1, and from EPSRC EP/S030468/1, EP/N010531/1. The authors would like to acknowledge Integrated Lab Solutions GmbH (ILS) for the design and manufacture of the high throughput reactor, and their continued support and technical expertise.

Declarations

Conflict of interest There are no conflicts to declare.

Open Access This article is licensed under a Creative Commons Attribution 4.0 International License, which permits use, sharing, adaptation, distribution and reproduction in any medium or format, as long as you give appropriate credit to the original author(s) and the source, provide a link to the Creative Commons licence, and indicate if changes were made. The images or other third party material in this article are included in the article's Creative Commons licence, unless indicated otherwise in a credit line to the material. If material is not included in the article's Creative Commons licence and your intended use is not permitted by statutory regulation or exceeds the permitted use, you will need to obtain permission directly from the copyright holder. To view a copy of this licence, visit <http://creativecommons.org/licenses/by/4.0/>.

References

- Zhong J, Yang X, Wu Z et al (2020) State of the art and perspectives in heterogeneous catalysis of CO₂ hydrogenation to methanol. *Chem Soc Rev* 49:1385–1413
- Golunski S, Burch R (2021) CO₂ hydrogenation to methanol over copper catalysts: learning from syngas conversion. *Top Catal* 1:3. <https://doi.org/10.1007/s11244-021-01427-y>
- Prašnikar A, Pavličič A, Ruiz-Zepeda F et al (2019) Mechanisms of copper-based catalyst deactivation during CO₂ reduction to methanol. *Ind Eng Chem Res* 58:13021–13029. <https://doi.org/10.1021/acs.iecr.9b01898>
- Fichtl MB, Schlereth D, Jacobsen N et al (2015) Kinetics of deactivation on Cu/ZnO/Al₂O₃ methanol synthesis catalysts. *Appl Catal A Gen* 502:262–270. <https://doi.org/10.1016/j.apcata.2015.06.014>
- Sun JT, Metcalfe IS, Sahibzada M (1999) Deactivation of Cu/ZnO/Al₂O₃ methanol synthesis catalyst by sintering. *Ind Eng Chem Res* 38:3868–3872. <https://doi.org/10.1021/ie990078s>
- Bahruji H, Bowker M, Hutchings G et al (2016) Pd/ZnO catalysts for direct CO₂ hydrogenation to methanol. *J Catal* 343:133–146. <https://doi.org/10.1016/j.jcat.2016.03.017>
- Bowker M, Lawes N, Gow I et al (2022) The critical role of βPdZn alloy in Pd/ZnO catalysts for the hydrogenation of carbon dioxide to methanol. *ACS Catal* 12:5371–5379. <https://doi.org/10.1021/acscatal.2c00552>
- Bahruji H, Bowker M, Jones W et al (2017) PdZn catalysts for CO₂ hydrogenation to methanol using chemical vapour impregnation (CVI). *Faraday Discuss* 197:309–324. <https://doi.org/10.1039/C6FD00189K>
- Ruiz Esquius J, Bahruji H, Taylor SH et al (2020) CO₂ hydrogenation to CH₃OH over PdZn catalysts, with reduced CH₄ production. *ChemCatChem* 12:6024–6032. <https://doi.org/10.1002/cctc.20200974>
- Bahruji H, Esquius JR, Bowker M et al (2018) Solvent free synthesis of PdZn/TiO₂ catalysts for the hydrogenation of CO₂ to methanol. *Top Catal* 61:144–153. <https://doi.org/10.1007/s11244-018-0885-6>
- Quilis C, Mota N, Pawelec B et al (2023) Intermetallic PdZn/TiO₂ catalysts for methanol production from CO₂ hydrogenation: the effect of ZnO loading on PdZn-ZnO sites and its influence on activity. *Appl Catal B Environ* 321:122064. <https://doi.org/10.1016/j.apcatb.2022.122064>
- Zabitskiy M, Sushkevich VL, Newton MA et al (2021) Mechanistic study of carbon dioxide hydrogenation over Pd/ZnO-based catalysts: the role of palladium-zinc alloy in selective methanol synthesis. *Angew Chemie Int Ed* 60:17053–17059. <https://doi.org/10.1002/anie.202103087>
- Fairley N, Fernandez V, Richard-Plouet M et al (2021) Systematic and collaborative approach to problem solving using X-ray photoelectron spectroscopy. *Appl Surf Sci Adv* 5:100112. <https://doi.org/10.1016/j.apsadv.2021.100112>
- Lawes N, Gow I, Smith LR et al (2022) Methanol synthesis from CO₂ and H₂ using supported Pd alloy catalysts. *Faraday Discuss*. <https://doi.org/10.1039/D2FD00119E>
- Malik AS, Zaman SF, Al-Zahrani AA et al (2018) Development of highly selective PdZn/CeO₂ and Ca-doped PdZn/CeO₂ catalysts for methanol synthesis from CO₂ hydrogenation. *Appl Catal A Gen* 560:42–53. <https://doi.org/10.1016/j.apcata.2018.04.036>
- Wilson NM, Schröder J, Priyadarshini P et al (2018) Direct synthesis of H₂O₂ on PdZn nanoparticles: the impact of electronic modifications and heterogeneity of active sites. *J Catal* 368:261–274. <https://doi.org/10.1016/j.jcat.2018.09.020>
- Hatta AH, Jalil AA, Hamid MYS et al (2023) The interparticle oxygen vacancies enrichment in the matrix of fibrous silica ceria

- supported nickel for CO methanation. *Fuel* 333:126539. <https://doi.org/10.1016/j.fuel.2022.126539>
18. Wang X, Shi H, Kwak JH, Szanyi J (2015) Mechanism of CO₂ hydrogenation on Pd/Al₂O₃ catalysts: kinetics and transient DRIFTS-MS studies. *ACS Catal* 5:6337–6349. <https://doi.org/10.1021/acscatal.5b01464>
 19. Araki M, Ponec V (1976) Methanation of carbon monoxide on nickel and nickel-copper alloys. *J Catal* 44:439–448. [https://doi.org/10.1016/0021-9517\(76\)90421-8](https://doi.org/10.1016/0021-9517(76)90421-8)
 20. Hu D, Gao J, Ping Y et al (2012) Enhanced investigation of CO methanation over Ni/Al₂O₃ catalysts for synthetic natural gas production. *Ind Eng Chem Res* 51:4875–4886. <https://doi.org/10.1021/ie300049f>
 21. Goguet A, Meunier FC, Tibiletti D et al (2004) Spectrokinetic investigation of reverse water-gas-shift reaction intermediates over a Pt/CeO₂ catalyst. *J Phys Chem B* 108:20240–20246. <https://doi.org/10.1021/jp047242w>
 22. Gallagher JR, Childers DJ, Zhao H et al (2015) Structural evolution of an intermetallic Pd–Zn catalyst selective for propane dehydrogenation. *Phys Chem Chem Phys* 17:28144–28153. <https://doi.org/10.1039/C5CP00222B>
 23. Forde MM, Kesavan L, Bin Saiman MI et al (2014) High activity redox catalysts synthesized by chemical vapor impregnation. *ACS Nano* 8:957–969. <https://doi.org/10.1021/nn405757q>
 24. Lee JY, Punkkinen MPJ, Schönecker S, Nabi Z, Kádas K, Zólyomi V, Koo YM, Hu QM, Ahuja R, Johansson B, Kollár J, Vitos L, Kwon SK (2018) The surface energy and stress of metals. *Surf Sci* 674:51–68. <https://doi.org/10.1016/j.susc.2018.03.008>

Publisher's Note Springer Nature remains neutral with regard to jurisdictional claims in published maps and institutional affiliations.